Mechanistic insights into electrocatalytic CO_2 reduction within $[Ru^{II}(tpy)(NN)X]^{n+}$ architectures

Travis A. White, Somnath Maji, and Sascha Ott*

Department of Chemistry, Ångström Laboratory, Uppsala Universitet, Box 523, 75120 Uppsala, Sweden.

Abstract

A series of Ru^{II}-polypyridyl complexes of the design $[Ru^{II}(tpy)(NN)X]^{n+}$ (tpy = 2,2′:6′,2″-terpyridine; NN = bidentate polypyridine; X = Cl^- or CH_3CN; n = 1 or 2) have been synthesized and analyzed for their ability to function as electrocatalysts in the reduction of CO_2 to CO. Varying the electron-donating/withdrawing character of the NN polypyridyl ligand has allowed for modification of electron density at the formally Ru^{II} metal center. Complexes where X = Cl^- display ligand substitution for CH_3CN with differing rates of Cl^- dissociation (k_{-Cl}), therefore providing a degree of insight into the electron density and thus the chemical activity at the Ru^{II} center. Detailed analysis of the cyclic voltammograms under argon vs. CO_2 atmospheres using multiple switching potentials and scan rates ranging from v = 25-2000 mV/s has painted a picture of how monodentate ligand lability due to NN polypyridyl electron-donating character is related to electrocatalytic CO_2 reduction activity of Ru^{II}-polypyridyl complexes. From these studies, multiple mechanistic pathways towards generating the catalytically active $[Ru(tpy^-)(NN^-)CO_2]^0$ species are proposed and differ *via* the order of electrochemical and chemical processes.

1 **Introduction**

2 High levels of thermodynamically stable, kinetically inert CO_2 within Earth's biosphere from

3 anthropogenic sources have forced the scientific community to develop a means for CO_2

4 fixation. Converting CO_2 to higher-energy species capable of providing energy in a fashion

5 similar to fossil fuels is of great interest and importance in the quest for alternative fuel sources.

6 An attractive approach to this issue involves the use of photochemical[1-4] and/or electrochemical[5,]

7 [6] reductive processes to convert CO_2 into CO, HCOOH, CH_3OH, or CH_4. Multi-electron/proton

8 transfer processes provide a lower thermodynamic potential compared to the one-electron

9 reduction which generates a high energetic $CO_2^{-\bullet}$ radical anion. Equations 1-6 show the

10 thermodynamic formal potential ($E^{o\prime}$) for each reductive process measured in V vs. NHE at 25 °C

11 in pH = 7 aqueous solution.[7]

12 $CO_2 + 1e^- \rightarrow CO_2^{-\bullet}$ $\qquad$ −1.90 V $\qquad$ (1)

13 $CO_2 + 2e^- + 2H^+ \rightarrow HCO_2H$ $\qquad$ −0.61 V $\qquad$ (2)

14 $CO_2 + 2e^- + 2H^+ \rightarrow CO + H_2O$ $\qquad$ −0.53 V $\qquad$ (3)

15 $CO_2 + 4e^- + 4H^+ \rightarrow H_2CO + H_2O$ $\qquad$ −0.48 V $\qquad$ (4)

16 $CO_2 + 6e^- + 6H^+ \rightarrow CH_3OH + H_2O$ $\qquad$ −0.38 V $\qquad$ (5)

17 $CO_2 + 8e^- + 8H^+ \rightarrow CH_4 + 2H_2O$ $\qquad$ −0.24 V $\qquad$ (6)
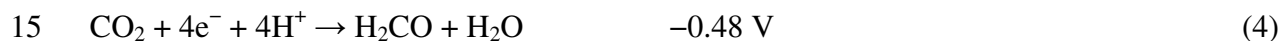
18 Transition metal-based catalysts are able to circumvent the energetically unfavorable $CO_2^{-\bullet}$

19 radical anion by providing a lower energy pathway for CO_2 reduction *via* multi-electron

20 processes. Of equal importance is the necessity for CO_2-selective reduction catalysts as protons

21 are able to be reduced to H_2 at potentials more negative than −0.41 V vs. NHE. Combining the

22 appropriate balance of electronics (provided by the ligand architecture) and the intrinsic

23 properties of the metal center has generated several molecular architectures incorporating

1 cyclams (Co[II], Ni[II])[7-10], porphyrins (Fe[0])[11, 12], phosphines (Rh[I], Pd[II], Ir[III])[13-16], and polypyridines

2 (Mn[I], Ru[II], Rh[III], Re[I], Ir[III])[17-29] that function as electrocatalysts for CO_2 reduction. The utilization

3 of electrochemical methods provides further insight into the factors that affect CO_2 reduction

4 (redox potentials, electron transfer rates, chemical kinetics) and assist in elucidating mechanistic

5 pathway(s) towards product formation. This powerful tool can therefore be used to not only

6 compare catalysts, but also contribute to the design of future, more efficient catalysts.

7 Polypyridine-containing molecular architectures present a subset of CO_2-reducing catalysts

8 that are of great interest given the ability to tune the electronics *via* ligand modification and the

9 potential to store multiple reducing equivalents within the polypyridyl scaffold.[23, 30] Molecular

10 architectures of type [Ru[II](NNN)(NN)X][n+] (where NNN = tridentate polypyridyl ligand, NN =

11 bidentate polypyridyl ligand, X = monodentate ligand) have recently been demonstrated to be

12 viable catalysts for H_2O oxidation[31-38], H_2O reduction[39], and CO_2 reduction[18, 21, 40, 41].

13 Incorporation of electron-donating or -withdrawing groups in the polypyridyl ligand is expected

14 to increase or decrease electron density at the formally Ru[II] reactive metal center, respectively,

15 and drive formation of specific products (i.e. Ru-hydrido, Ru-carboxylato, Ru-formato) in the

16 presence of various educts (i.e. H^{−}, H^{+}, CO_2, H_2O). As one might expect, the rate of product

17 formation should also be affected by electron density at the Ru[II] center. While numerous studies

18 have been performed to assess the impact polypyridyl ligand modification has on H_2O oxidation,

19 surprisingly few studies report the role polypyridyl ligand modification has on CO_2 reduction

20 within a Ru[II] architecture.[21, 40]

21 Reported herein are the electrochemical properties and electrocatalytic activity for a series of

22 [Ru[II](tpy)(NN)X][n+] complexes **1-6** (NN = bidentate polypyridyl ligand; X = monodentate ligand)

23 with varying degrees of electron-donating/withdrawing capabilities within the bidentate ligand

1   set, **Figure 1**. A thorough and systematic approach to understanding the observed

2   electrochemical processes provides insight into the electrocatalytic activity towards CO_2

3   reduction and generates a picture of the factors impacting catalysis. Complexes where X = Cl$^-$

4   (labeled [Ru^{II}-Cl]$^+$) provide a probe into monodentate ligand lability at the Ru^{II} center as a

5   function of bidentate ligand electron-donating ability and are found to correlate with the

6   observed trend for CO_2 reduction activity. Similarly, complexes where X = CH$_3$CN (labeled

7   [Ru^{II}-NCCH$_3$]$^{2+}$) serve as not only reference complexes for deciphering electrochemical

8   mechanisms within [Ru^{II}-Cl]$^+$ complexes, but also to confirm observed trends in electrocatalytic

9   CO_2 reduction using various bidentate ligands. Electrochemical studies further suggest that CO_2

10   binding can occur at the one-electron reduced [Ru^{II}-Cl]^0 level or the two-electron reduced [Ru^{II}-

11   NCCH$_3$]^0 level when bidentate ligands with electron-donating character are incorporated.

[Ru^{II}(tpy)(Me$_2$bpy)X]$^{n+}$
1-Cl, 1-CH$_3$CN

[Ru^{II}(tpy)(^{t}Bu$_2$bpy)X]$^{n+}$
2-Cl, 2-CH$_3$CN

[Ru^{II}(tpy)((MeO)$_2$bpy)X]$^{n+}$
3-Cl, 3-CH$_3$CN

[Ru^{II}(tpy)(phen)X]$^{n+}$
4-Cl, 4-CH$_3$CN

[Ru^{II}(tpy)(bpm)X]$^{n+}$
5-Cl, 5-CH$_3$CN

[Ru^{II}(tpy)(dppz)X]$^{n+}$
6-Cl, 6-CH$_3$CN

X = Cl;   n = 1
X = CH$_3$CN; n = 2
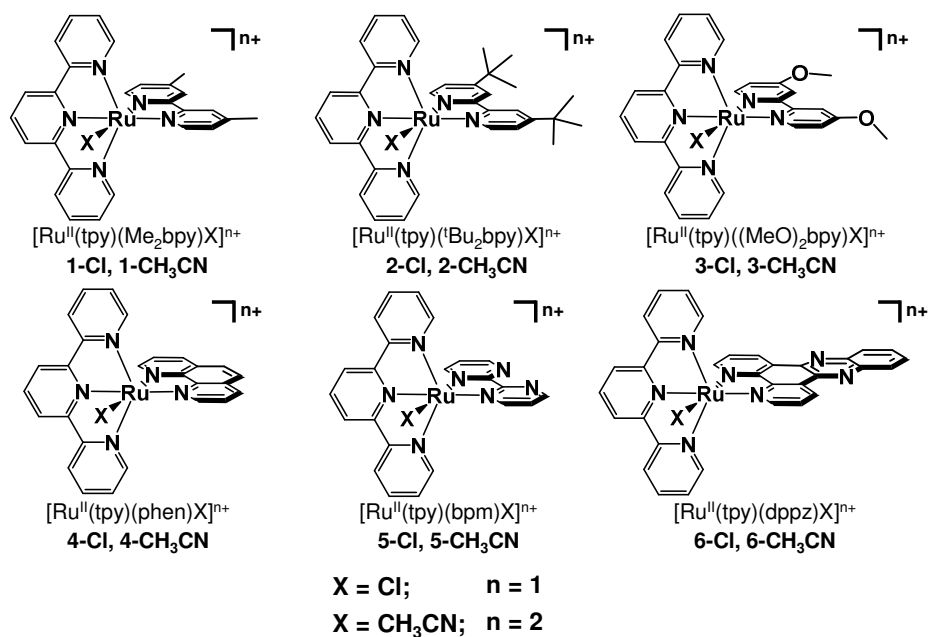
12

13   **Fig. 1** Structures of Ru^{II}-polypyridyl complexes for electrocatalytic CO_2 reduction in this study.

14   **Experimental Section**

1   **Materials.** All solvents were reagent grade and all materials were used as received unless

2   otherwise stated. RuCl$_3$•3H$_2$O and triethylamine (TEA) were purchased from Acros Organics.

3   2,2′:6′,2″-Terpyridine (tpy), 4,4′-Di-*tert*-butyl-2,2′-bipyridine (4,4′-^{t}Bu$_2$bpy), and lithium

4   chloride were purchased from Sigma-Aldrich. 4,4′-Dimethyl-2,2′-bipyridine (4,4′-Me$_2$bpy), 4,4′-

5   dimethoxy-2,2′-bipyridine (4,4′-(MeO)$_2$bpy), 1,10-phenanthroline (phen), and 2,2′-bipyrimidine

6   (bpm) were purchased from Aldrich. Ammonium hexafluorophosphate and tetrabutylammonium

7   hexafluorophosphate ($\geq$ 99.0%) were purchased from Fluka. CO$_2$(g) (99.998%) was purchased

8   from Air Liquide. Glassware used for electrochemical analyses were kept in a 120°C oven until

9   needed.

10   The bidentate ligand dipyrido[3,2-a:2′,3′-c]phenazine (dppz)[42], [Ru^{III}(tpy)Cl$_3$][43],

11   [Ru^{II}(tpy)(4,4′-Me$_2$bpy)Cl](PF$_6$) (**1-Cl**)[44], [Ru^{II}(tpy)(4,4′-^{t}Bu$_2$bpy)Cl](PF$_6$) (**2-Cl**)[38],

12   [Ru^{II}(tpy)(4,4′-(MeO)$_2$bpy)Cl](PF$_6$) (**3-Cl**)[40], [Ru^{II}(tpy)(phen)Cl](PF$_6$) (**4-Cl**)[45],

13   [Ru^{II}(tpy)(bpm)Cl](PF$_6$) (**5-Cl**)[46], [Ru^{II}(tpy)(dppz)Cl](PF$_6$) (**6-Cl**)[47],

14   [Ru^{II}(tpy)(phen)NCCH$_3$](PF$_6$)$_2$ (**4-CH$_3$CN**)[45], [Ru^{II}(tpy)(bpm)NCCH$_3$](PF$_6$)$_2$ (**5-CH$_3$CN**)[46] and

15   [Ru^{II}(tpy)(dppz)NCCH$_3$](PF$_6$)$_2$ (**6-CH$_3$CN**)[48] were synthesized as previously reported.

16   **[Ru^{II}(tpy)(4,4′-Me$_2$bpy)NCCH$_3$](PF$_6$)$_2$ (1-CH$_3$CN).** [Ru^{II}(tpy)(4,4′-Me$_2$bpy)Cl](PF$_6$) (0.081

17   g, 0.12 mmol) was heated at reflux in the dark overnight using 1:1 CH$_3$CN/H$_2$O (50 mL). The

18   orange solution was cooled to room temperature and the volume reduced to ~20 mL which

19   induced precipitation of an orange solid. Additional orange precipitate formed upon adding ~15

20   mL of 0.2 M NH$_4$PF$_6$(aq). The precipitate was filtered and washed with cold water and diethyl

21   ether to yield a bright orange solid (0.064 g, 0.075 mmol, yield = 65%). Elemental analysis

22   calculated for C$_{29}$H$_{26}$F$_{12}$N$_6$P$_2$Ru•1H$_2$O: C, 40.15; H, 3.25; N, 9.69. Found: C, 40.41; H, 3.24; N,

23   9.66. ^{1}H-NMR (400 MHz, CD$_3$CN) δ 9.39 (d, *J* = 5.7 Hz, 1H), 8.53 (d, *J* = 8.1 Hz, 2H), 8.47 (s,

1H), 8.40 (d, J = 8.1 Hz, 2H), 8.27 (t, J = 8.1 Hz, 1H), 8.21 (s, 1H), 7.99 (td, J = 7.9, 1.5 Hz,

2H), 7.79 (dd, J = 5.7, 1.2 Hz, 1H), 7.70 – 7.66 (m, 2H), 7.39 – 7.31 (m, 2H), 7.06 (d, J = 5.8 Hz,

1H), 6.90 (dd, J = 6.1, 1.3 Hz, 1H), 2.75 (s, 3H), 2.36 (s, 3H). ESI-MS(+): $[M-PF_6]^+$, m/z =

703.8 (calc: m/z = 704.6); $[M-2PF_6]^{2+}$, m/z = 279.5 (calc: m/z = 279.8).

$[Ru^{II}(tpy)(4,4'-{}^tBu_2bpy)NCCH_3](PF_6)_2$ (2-CH₃CN). The same procedure for the $[Ru^{II}(tpy)(4,4'-Me_2bpy)NCCH_3](PF_6)_2$ was followed using $[Ru^{II}(tpy)(4,4'-{}^tBu_2bpy)Cl](PF_6)$ (0.081 g, 0.10 mmol) to yield a bright orange solid (0.050 g, 0.054 mmol, yield = 52%). Elemental analysis calculated for $C_{35}H_{38}F_{12}N_6P_2Ru \cdot 1H_2O$: C, 44.17; H, 4.24; N, 8.83. Found: C, 44.11; H, 4.22; N, 8.82. ^{1}H-NMR (400 MHz, CD₃CN) δ 9.44 (d, J = 6.0 Hz, 1H), 8.59 (d, J = 2.0 Hz, 1H), 8.54 (d, J = 8.2 Hz, 2H), 8.41 (d, J = 8.1 Hz, 2H), 8.33 (d, J = 1.9 Hz, 1H), 8.31 – 8.25 (m, 1H), 8.00 (td, J = 7.9, 1.5 Hz, 2H), 7.94 (dd, J = 6.0, 2.0 Hz, 1H), 7.71 – 7.65 (m, 2H), 7.36 (ddd, J = 7.6, 5.5, 1.3 Hz, 2H), 7.11 (d, J = 6.1 Hz, 1H), 7.05 (dd, J = 6.1, 2.1 Hz, 1H), 1.60 (s, 9H), 1.25 (s, 9H). ESI-MS(+): $[M-PF_6]^+$, m/z = 787.8 (calc: m/z = 788.8); $[M-2PF_6]^{2+}$, m/z = 321.3 (calc: m/z = 321.9).

$[Ru^{II}(tpy)(4,4'-(MeO)_2bpy)NCCH_3](PF_6)_2$ (3-CH₃CN). The same procedure for the $[Ru^{II}(tpy)(4,4'-Me_2bpy)NCCH_3](PF_6)_2$ was followed using $[Ru^{II}(tpy)(4,4'-(MeO)_2bpy)Cl](PF_6)$ (0.070 g, 0.095 mmol) to yield a bright orange solid (0.054 g, 0.061 mmol, yield = 64%). Elemental analysis calculated for $C_{29}H_{26}F_{12}N_6O_2P_2Ru \cdot 1H_2O$: C, 38.72; H, 3.14; N, 9.34. Found: C, 38.52; H, 3.10; N, 9.18. ^{1}H-NMR (400 MHz, CD₃CN) δ 9.32 (d, J = 6.4 Hz, 1H), 8.52 (d, J = 8.1 Hz, 2H), 8.40 (d, J = 8.1 Hz, 2H), 8.25 (t, J = 8.1 Hz, 1H), 8.13 (d, J = 2.7 Hz, 1H), 7.99 (td, J = 7.9, 1.5 Hz, 2H), 7.87 (d, J = 2.8 Hz, 1H), 7.78 – 7.72 (m, 2H), 7.52 (dd, J = 6.5, 2.7 Hz, 1H), 7.37 (ddd, J = 7.6, 5.5, 1.3 Hz, 2H), 6.97 (d, J = 6.6 Hz, 1H), 6.61 (dd, J = 6.6, 2.8 Hz, 1H),

1   4.18 (s, 3H), 3.83 (s, 3H). ESI-MS(+): $[M-PF_6]^+$, m/z = 735.7 (calc: m/z = 736.6); $[M-2PF_6]^{2+}$,

2   m/z = 295.1 (calc: m/z = 295.8).

3   **Physical Measurements.** ^{1}H-NMR spectra were measured in CD_3CN solvent using a JEOL

4   400 MHz spectrometer at 293 K. The chemical shifts given in ppm are internally referenced to

5   the residual CH_3CN solvent signal (1.96 ppm).[49] HPLC-MS data were obtained using a Dionex

6   UltiMate 3000 system on a Phenomenex Gemini C18 column (150 x 3.0 mm, 5μm) coupled to a

7   Thermo LCQ Deca XP Max with electrospray ionization. Solvents used for HPLC: 0.05%

8   HCO_2H in H_2O and 0.05% HCO_2H in CH_3CN. Electronic absorption spectra were measured in

9   CH_3CN solvent using a Varian Cary 50 UV-Vis spectrophotometer with 1 nm resolution.

10   Elemental analysis (C,H,N) was performed by Analytische Laboratorien GmbH (Lindlar,

11   Germany).

12   **Electrochemistry.** Cyclic voltammetry (CV) experiments were performed using a one-

13   compartment, three-electrode configuration connected to an Autolab PGSTAT100 potentiostat

14   controlled with GPES 4.9 software (EcoChemie). The electrode setup included a glassy carbon

15   disc (0.071 cm^2) working electrode that was polished using 0.05 μM alumina prior to use, a

16   carbon rod auxiliary electrode, and a Ag/Ag$^+$ (0.01 M AgNO$_3$ in CH_3CN, −0.060 V vs. Fc$^{0/+}$; Fc

17   = $[Fe(C_5H_5)_2]$) non-aqueous reference electrode. Potential values were converted to versus Fc$^{0/+}$

18   by addition of 60 mV. CVs containing 1 mM of each complex were measured using 0.1 M

19   Bu$_4$NPF$_6$ supporting electrolyte in either argon- or CO_2-saturated CH_3CN solutions at room

20   temperature with scan rates (ν) varying from 25 to 2000 mV/s. Rate constants for Cl$^-$

21   dissociation (k_{-Cl}) were obtained by fitting experimental CVs with simulated CVs using

22   DigiElch^{TM} 7 electrochemical simulation software. Overlaid simulated and experimental CVs for

1 complex **3-Cl**, along with the fitting parameter conditions, are shown in **Figure S5** in Supporting

2 Information to provide as an example.

3 **Bulk Electrolysis.** Bulk electrolysis experiments were performed using a one-compartment

4 cell, three-electrode configuration which comprised a glassy carbon rod (3.67 cm^2) working

5 electrode, carbon cloth auxiliary electrode, and Ag/Ag$^+$ (0.01 M AgNO$_3$ in CH$_3$CN, −0.060 V vs.

6 Fc$^{0/+}$) reference electrode controlled by the Autolab PGSTAT100 potentiostat. Experimental

7 conditions involved purging 0.1 M Bu$_4$NPF$_6$/CH$_3$CN solution (10 mL) containing 1 mM of

8 [Ru^{II}(tpy)(4,4′-Me$_2$bpy)(NCCH$_3$)]$^{2+}$ (**1-CH$_3$CN**) with CO$_2$ for 30 minutes prior to applying a

9 constant potential of −2.04 V vs. Fc$^{0/+}$, providing a [CO$_2$] = 0.28 M.[50] Gas samples were

10 analyzed using a Perkin Elmer Clarus 500 series gas chromatogram (GC) equipped with a

11 thermal conductivity detector (TCD), stainless-steel column packed with molecular sieves (60/80

12 mesh), and N$_2$ as the carrier gas (flow rate = 35 mL/min). The operating temperatures of the

13 injection port, the oven/column, and detector were 100°C, 80°C, and 100°C, respectively.

14 Aliquots (250 μL) of the gas headspace were injected into the GC after 10 min electrolysis to

15 analyze the gas products formed.

16 **Results and Discussion**

17 **Synthesis.** The Ru^{II}-polypyridyl complexes were synthesized (**Scheme 1**) *via* step-wise

18 reactions whereby the tridentate tpy ligand was first coordinated to RuCl$_3$•3H$_2$O, followed by

19 bidentate ligand coordination to afford [Ru(tpy)(NN)Cl](PF$_6$) as dark maroon/purple solids.

20 Converting the Cl$^-$ substituted complexes to CH$_3$CN substitution was achieved by heating the

21 complexes at reflux in CH$_3$CN/H$_2$O mixtures to afford [Ru(tpy)(NN)NCCH$_3$](PF$_6$)$_2$ as orange

22 solids. Isotopic distribution patterns, obtained using ESI-MS operating in positive mode, were in

1 agreement with calculated spectra as mass-to-charge ratios displayed $[M-PF_6]^+$ and $[M-2PF_6]^{2+}$

2 for the newly reported $[Ru(tpy)(4,4'-Me_2bpy)NCCH_3](PF_6)_2$ (**1-CH$_3$CN**), $[Ru(tpy)(4,4'-$

3 $^tBu_2bpy)NCCH_3](PF_6)_2$ (**2-CH$_3$CN**), and $[Ru(tpy)(4,4'-(MeO)_2bpy)NCCH_3](PF_6)_2$ (**3-CH$_3$CN**)

4 complexes.

5

6 **Scheme 1** Synthetic scheme for the step-wise assembly of $[Ru^{II}(tpy)(NN)X]^{n+}$ complexes.
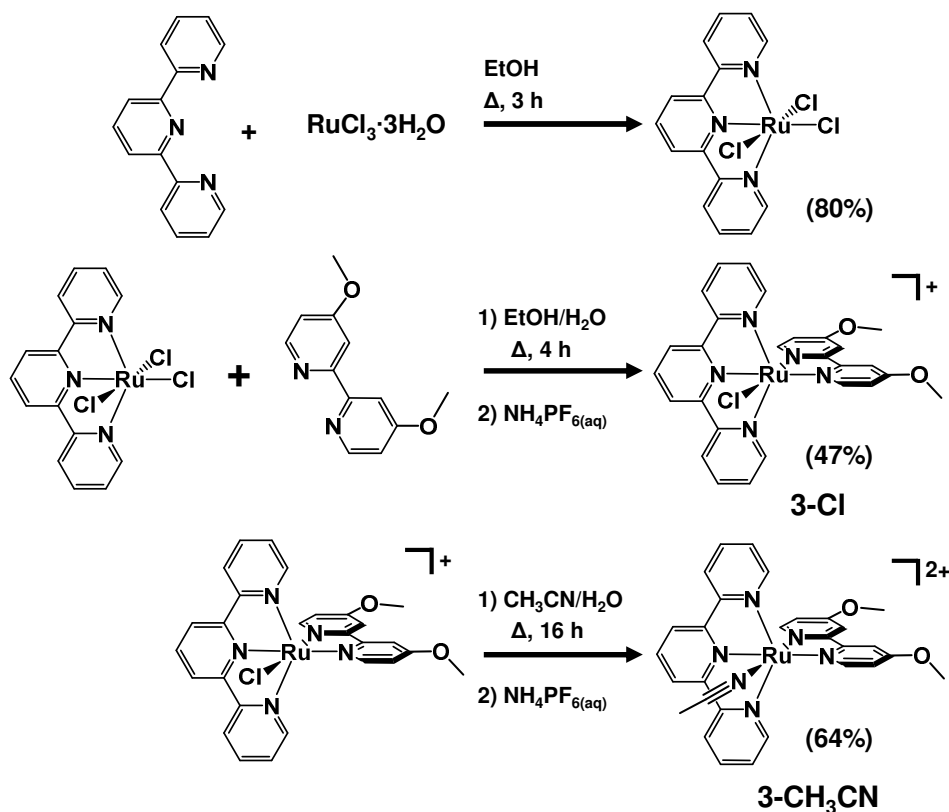
7 **Electrochemical Properties.** Electrochemistry provides insight into the redox-active nature

8 of $[Ru^{II}(tpy)(NN)X]^{n+}$ complexes, their electron affinities and chemical stability(**Figure 2;**

9 **Figures S6-S11**). The redox potentials of electrochemical processes are summarized in **Table 1**

10 and displayed in **Figure 3**. Anodic scans display a reversible, one-electron $Ru^{II/III}$ oxidation that

11 is strongly influenced by the nature of the monodentate ligand (Cl⁻ vs. CH$_3$CN) and, to a lesser

12 degree, the electron-donating/withdrawing ability of the bidentate ligand set. The $[Ru^{II}-Cl]^+$

1   complexes are oxidized at fairly mild potentials (+0.44 V to +0.66 V vs. Fc$^{0/+}$), with the

2   complexes containing electron-donating ligands (**1-Cl**, **2-Cl**, **3-Cl**) being easier to oxidize than

3   those containing electron-withdrawing ligands (**5-Cl**, **6-Cl**). This trend is expected as increased

4   electron density at Ru^{II} shifts the Ru-based HOMO to higher energy. Substituting the stronger π-

5   donor Cl$^−$ by a weaker π-donor CH$_3$CN to generate [Ru^{II}-NCCH$_3$]$^{2+}$ species stabilizes the Ru(dπ)

6   orbital set. Consequently, Ru$^{II/III}$ couple is observed at ~0.50 V more positive potentials,

7   indicative of a decrease in electron density at the Ru center.

8

9
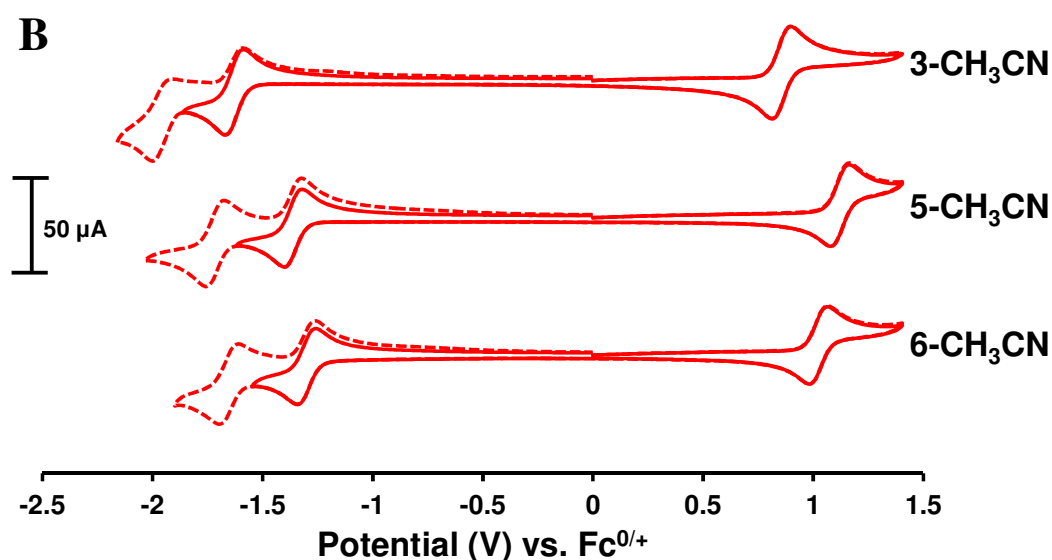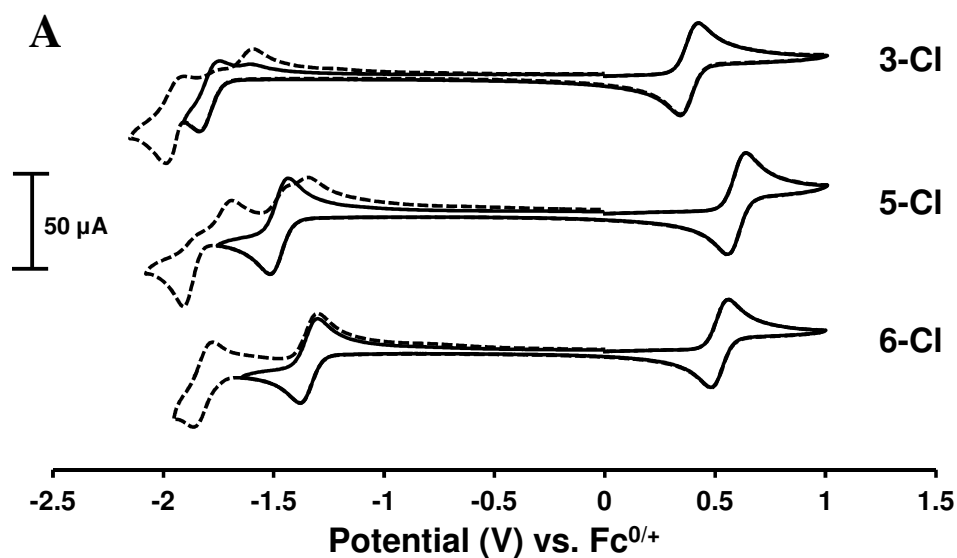
1   **Fig. 2** Cyclic voltammograms of 1 mM solutions of $[Ru^{II}(tpy)(NN)Cl]^+$ (**A**) and
2   $[Ru^{II}(tpy)(NN)NCCH_3]^{2+}$ (**B**) complexes (NN = 4,4′-(MeO)$_2$-bpy, bpm, or dppz) in Ar-saturated
3   CH_3CN using 0.1 M Bu$_4$NPF$_6$ supporting electrolyte at ν = 200 mV/s.

4

5   **Fig. 3** Reduction and oxidation potentials of $[Ru^{II}(tpy)(NN)X]^{n+}$ complexes (NN = bidentate
6   ligand; X = Cl$^-$ or CH$_3$CN). Energy values represent measured E$_{1/2}$ potentials which were
7   obtained using cyclic voltammetry. Black and red lines correspond to complexes where X = Cl$^-$
8   and CH$_3$CN, respectively.

9   **Table 1** Redox Potentials for $[Ru^{II}(tpy)(NN)X]^{n+}$ Complexes[a]

Complex	$[Ru\text{-}X]^{(n+1)/n}$ E$_{1/2}$, V (ΔE$_p$, mV)	$[Ru\text{-}X]^{n/(n-1)}$ E$_{1/2}$, V (ΔE$_p$, mV)	$[Ru\text{-}X]^{(n-1)/(n-2)}$ E$_{1/2}$, V (ΔE$_p$, mV)	k_{-Cl}[c] (s^{-1})
1-Cl	0.502 (82)	−1.709 (91)	[b]	1.1
1-CH$_3$CN	0.996 (90)	−1.546 (81)	−1.882 (110)	
2-Cl	0.511 (83)	−1.696 (82)	[b]	0.60
2-CH$_3$CN	0.985 (91)	−1.555 (73)	−1.884 (95)	
3-Cl	0.443 (81)	−1.731 (94)	[b]	0.45
3-CH$_3$CN	0.855 (90)	−1.573 (81)	−1.896 (101)	
4-Cl	0.547 (77)	−1.690 (84)	[b]	0.20
4-CH$_3$CN	1.055 (81)	−1.537 (81)	−1.838 (72)	

5-Cl	0.659 (81)	−1.412 (84)	−1.811 (79)	1×10^{-3}
5-CH₃CN	1.181 (81)	−1.303 (81)	−1.658 (72)	
6-Cl	0.582 (80)	−1.280 (79)	−1.759 (87)	5×10^{-4}
6-CH₃CN	1.082 (81)	−1.240 (81)	−1.600 (81)	

1   ^{a} Measurements performed using 1 mM of Ru^{II} complex in an argon-saturated CH₃CN solution with 0.1

2   M Bu₄NPF₆ supporting electrolyte at v = 200 mV/s. Values reported are measured vs. Fc$^{0/+}$. Values in

3   parentheses correspond to the cathodic and anodic peak potential separation for each redox couple. The

4   value of n = 1+ and 2+ for X = Cl$^−$ and CH₃CN complexes, respectively. ^{b} Reduction corresponding to

5   [Ru^{II}-Cl]$^{0/−}$ is not observed up to 2000 mV/s, only reduction for CH₃CN-substituted species. ^{c} Rate

6   constant for Cl$^−$ dissociation following first reduction of [Ru^{II}-Cl]$^+$ complexes calculated using

7   DigiElch^{TM} 7 software by fitting experimental CVs with simulated CVs.

8   Cathodic scans under an argon atmosphere present varied electrochemical properties

9   throughout the [Ru^{II}-Cl]$^+$ and [Ru^{II}-NCCH₃]$^{2+}$ series that are strongly influenced by bidentate

10   ligand identity. Each series of complexes possess sequential, one-electron, ligand-based

11   reductions with NN = Me₂bpy, ^{t}Bu₂bpy, (MeO)₂bpy, and phen complexes **1-4** possessing a

12   tpy(π*)-based first reduction. Conversely, NN = bpm and dppz complexes **5** and **6** possess a

13   NN(π*)-based first reduction due to the strong electron-accepting capability of the pyrimidine

14   and phenazine subunits. This orbital inversion assignment is supported by comparing the 1st

15   reduction potential of the respective tris homoleptic complexes (E$_{1/2}$([Ru(tpy)₂]$^{2+/+}$) = −1.67 V

16   vs. Fc$^{0/+}$; E$_{1/2}$([Ru(bpm)₃]$^{2+/+}$) = −1.38 V vs. Fc$^{0/+}$; E$_{1/2}$([Ru(dppz)₃]$^{2+/+}$) = −1.35 V vs. Fc$^{0/+}$)[51-53],

17   as well as a previously reported assignment for [Ru^{II}(tpy)(bpm)Cl](PF₆).[46] Switching scan

18   direction following the first reduction displays the chemical reactivity in [Ru^{II}-Cl]$^+$ complexes **1-**

19   **Cl** to **4-Cl**. As representatively shown in **Figure 4A**, the reverse scan in the CV of

20   [Ru^{II}(tpy)(4,4′-(MeO)₂bpy)Cl]$^+$ (**3-Cl**) displays two anodic waves (E$_p^a$), one at −1.68 V for the

21   expected [Ru^{II}-Cl]$^{0/+}$ oxidation, and a second oxidation at −1.53 V for the ligand-exchanged

22   [Ru^{II}-NCCH₃]$^{+/2+}$ oxidation. Similar chemical reactivity is observed for NN = Me₂bpy, ^{t}Bu₂bpy,

23   and phen complexes, **Figure S12**. Varying the scan rate from 25-2000 mV/s allows for

1   measuring the rate of Cl⁻ dissociation (k_{-Cl}) within these systems, providing a degree of insight

2   into monodentate ligand lability as a function of electron-donating ability from the bidentate

3   ligand to the formally Ru[II] metal center. DigiElch[TM] 7 electrochemical simulation software was

4   used to generate simulated CVs and fit those with experimentally obtained CVs by varying

5   parameters such as the reduction potential (E), the rate constant for heterogeneous electron

6   transfer (k_s), and the equilibrium constant and rate constant for a chemical reaction (i.e. Cl⁻

7   dissociation). The calculated k_{-Cl} values range from 5 x 10^{-4} to 1.1 s⁻¹ depending on electron-

8   donating character of the bidentate ligand, **Table 1**. Chloride ligand lability is not observed in the

9   one-electron reduced bpm or dppz-containing [Ru[II]-Cl]⁺ complexes **5-Cl** and **6-Cl** (**Figure 4B**

10   **and Figure S12,** respectively) in which the injected electron is localized on the electron-

11   deficient bidentate ligands that are evidently electronically isolated from the Ru-Cl bond. The

12   decreased electron density at Ru[II] of **5** and **6** suppresses Cl– ligand dissociation at the applied

13   potentials and therefore predicts **5** and **6** to function poorly as efficient catalysts for metal-

14   centered, reductive catalysis. [Ru[II]-NCCH₃]²⁺ complexes, regardless of bidentate ligand identity,

15   display a reversible one-electron, ligand(π*)-based reduction as CH₃CN dissociation is slow on

16   the electrochemical time scale at the applied potentials (**Figure S13**). The potential difference

17   between the anodic and cathodic waves ($\Delta E_p \approx 80$ mV) and the ratio of anodic to cathodic

18   current ($i_p^a/i_p^c \approx 0.9$) remain constant at all measured scan rates, indicating electrochemical and

19   chemical reversibility within [Ru[II]-NCCH₃]²⁺ complexes. When comparing $\Delta E_{1/2}$ values between

20   [Ru[II]-Cl]⁺/⁰ and [Ru[II]-NCCH₃]²⁺/⁺, the $E_{1/2}$ shifts to more positive potential by ~110-160 mV upon

21   CH₃CN coordination for all complexes except NN = dppz. The observed $\Delta E_{1/2}$ value of only 40

22   mV indicates the very strong electron-withdrawing nature of the phenazine component, as

1   CH₃CN substitution has a minimal affect and suggests some degree of electronic isolation

2   between the bipyridine and phenazine portions of the dppz ligand.
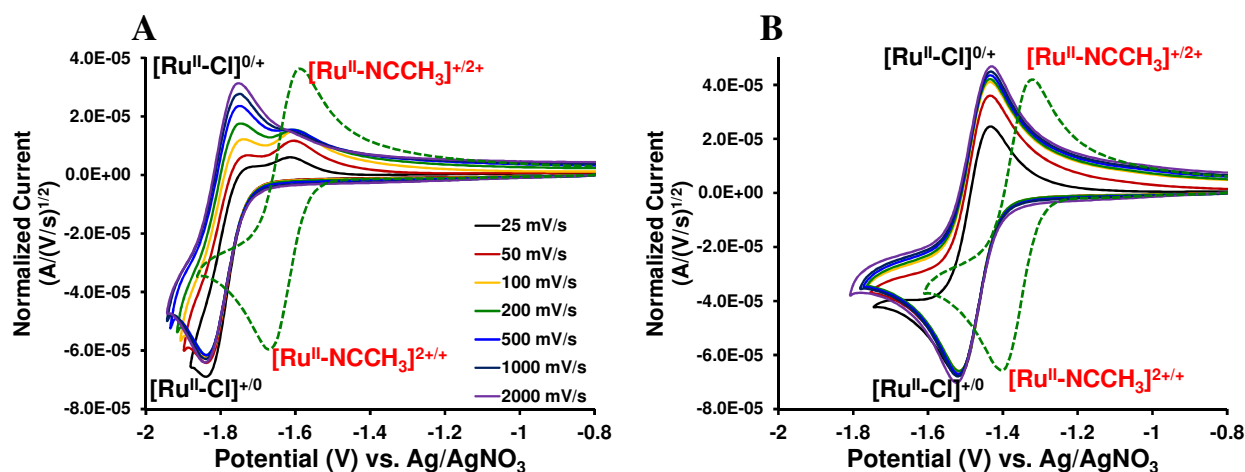
3

4   **Fig. 4** Cyclic voltammograms of $[Ru^{II}(tpy)(4,4'-(MeO)_2bpy)Cl]^+$, **3-Cl** (**A**) and

5    $[Ru^{II}(tpy)(bpm)Cl]^+$, **5-Cl** (**B**) complexes with v ranging from 25 mV/s (black line) to 2000 mV/s

6   (purple line). The 1ˢᵗ reduction at v = 200 mV/s (green dashed line) for $[Ru^{II}(tpy)(4,4'-$

7    $(MeO)_2bpy)NCCH_3]^{2+}$, **3-CH₃CN** (**A**) and $[Ru^{II}(tpy)(bpm)NCCH_3]^{2+}$, **5-CH₃CN** (**B**) complexes

8   are included as a reference. $[Ru^{II}-Cl]$ and $[Ru^{II}-NCCH_3]$ labels correspond to the presence of Cl^-

9   or CH₃CN bound species.

10   Continued cathodic scanning presents further varied electrochemical properties and chemical

11   reactivity. $[Ru^{II}-Cl]^+$ complexes **1-Cl** to **4-Cl** do not display a $[Ru^{II}-Cl]^{0/-}$ reduction under argon

12   due to Ru-Cl bond labilization and CH₃CN coordination upon further applied negative bias.

13   Therefore, only the reduction corresponding to $[Ru^{II}-NCCH_3]^{+/0}$ is observed, **Figure 5A** and

14   **Figure S14**. As expected, return anodic scans display only re-oxidations that arise from the

15   CH₃CN-bound complexes. Electron-withdrawing ligands as in **5-Cl** and **6-Cl** stabilize the $[Ru^{II}-$

16    $Cl]^0$ species which exhibit a $[Ru^{II}-Cl]^{0/-}$ reduction that is tpy(π^*)-based at E_p^c = −1.85 V (bpm)

17   and −1.80 V (dppz). For **5-Cl**, two-electron reduction forms $[Ru^{II}(\mathbf{tpy}^-)(\mathbf{bpm}^-)Cl]^-$ which is

18   quasi-stable as the presence of both $[Ru^{II}-Cl]^{-/0}$ and $[Ru^{II}-NCCH_3]^{0/+}$ re-oxidations are observed

19   at E_p^a = −1.77 V and −1.62 V, respectively, **Figure 5B**. Re-oxidation of both one-electron

14

1   reduced species, $[Ru^{II}\text{-}Cl]^{0/+}$ and $[Ru^{II}\text{-}NCCH_3]^{+/2+}$, is only observed when the potential has been

2   scanned past two reductive couples, indicating that Ru-Cl bond labilization for NN = bpm

3   requires two electrons. Complex **6-Cl** is able to undergo two-electron reduction to form

4    $[Ru^{II}(\mathbf{tpy^-})(\mathbf{dppz^-})Cl]^-$ with the Cl^- ligand remaining coordinated to Ru^{II} at v = 200 mV/s

5   (**Figure 2A**). This lack of Cl^- lability emphasizes the impact strongly electron-withdrawing

6   ligands have on chemical reactivity at the sixth coordination site within this architecture which

7   requires ligand dissociation prior to formation of a catalytically active species. Assignments for

8   each redox couple within the Cl^- series of complexes are justified by using the synthesized

9    $[Ru^{II}(tpy)(NN)NCCH_3]^{2+}$ complexes as a reference given the observed redox couples will only

10   correspond to $[Ru^{II}\text{-}NCCH_3]$ species.
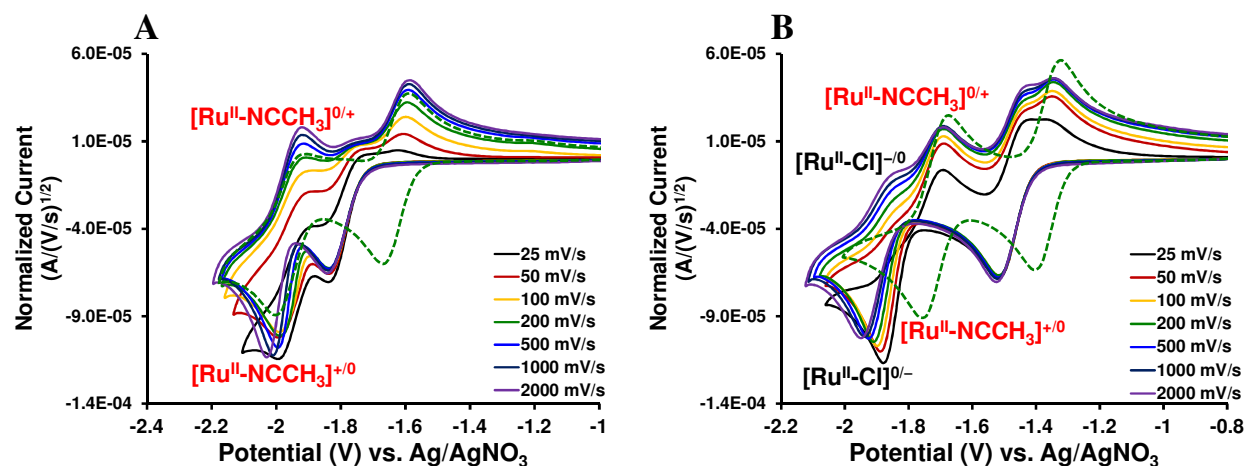
11

12   **Fig. 5** Cyclic voltammograms (including the 2nd reduction) of $[Ru^{II}(tpy)(4,4'\text{-}(MeO)_2bpy)Cl]^+$, **3-**

13   **Cl** (**A**) and $[Ru^{II}(tpy)(bpm)Cl]^+$, **5-Cl** (**B**) complexes with v ranging from 25 mV/s (black line) to

14   2000 mV/s (purple line). The CVs of $[Ru^{II}(tpy)(4,4'\text{-}(MeO)_2bpy)NCCH_3]^{2+}$, **3-CH$_3$CN** (**A**) and

15   $[Ru^{II}(tpy)(bpm)NCCH_3]^{2+}$, **5-CH$_3$CN** (**B**) at v = 200 mV/s (green dashed line) are included as a

16   reference. $[Ru^{II}\text{-}Cl]$ and $[Ru^{II}\text{-}NCCH_3]$ labels correspond to the presence of Cl^- or CH_3CN bound

17   species.

1   While the synthesized [Ru^{II}-NCCH$_3$] complexes are expected to display chemical stability

2   upon multi-electron reduction, two trends were observed. The complexes containing NN = bpm

3   (**5-CH$_3$CN**) or dppz (**6-CH$_3$CN**) displayed two reversible, one-electron reductions (**Figure S15**).

4   However, complexes where NN = Me$_2$bpy (**1-CH$_3$CN**), ^{t}Bu$_2$bpy (**2-CH$_3$CN**), or (MeO)$_2$bpy (**3-**

5   **CH$_3$CN**) deviate substantially from chemical reversibility for the second reduction as CH$_3$CN

6   dissociation is observed at scan rates as low as 200 mV/s (**Figure S15**). This assignment is in

7   direct agreement with a previous observation for [Ru^{II}(tpy)(bpy)NCCH$_3$]$^{2+}$.[54] Substitution of

8   CH$_3$CN for a substrate, such as CO$_2$, is therefore expected to be favorable due to ligand lability

9   at the sixth coordination site in complexes containing electron-donating substituents (methoxy,

10   *tert*-butyl, or methyl). Complexes containing strong, electron-withdrawing subunits (pyrimidines

11   or phenazines) are expected to display minimal-to-negligible reactivity towards CO$_2$ substitution

12   as ligand reduction does not greatly labilize the Ru-X bond. Complexes where NN = phen (**4-Cl**

13   and **4-CH$_3$CN**) present an intermediary regime as the phenanthroline ligand contains appropriate

14   electron-donating ability to labilize the Ru-Cl bond upon one-electron reduction for [Ru^{II}-Cl]$^+$,

15   but also possesses sufficient electron-withdrawing character to minimize CH$_3$CN dissociation

16   upon two-electron reduction for [Ru^{II}-NCCH$_3$]$^{2+}$ complexes (**Figure S15**).

17   **Electrocatalytic Properties.** Cyclic voltammograms were obtained under a CO$_2$ atmosphere

18   to assess the capabilities of [Ru^{II}(tpy)(NN)X]$^{n+}$ complexes for electrocatalytic CO$_2$ reduction.

19   Bulk electrolysis of a CO$_2$-saturated solution of **1-CH$_3$CN** was performed and the headspace

20   analyzed by gas chromatography to confirm the formation of CO as the major product, **Figure**

21   **S16**, as well as measuring reference gas samples to identify retention times. Anodic scans did not

22   alter the redox-active nature, chemical stability, or potential of the $Ru^{II/III}$ couple in any

23   complexes, indicating that Cl$^-$ or CH$_3$CN do not dissociate at applied positive bias and CO$_2$ is

1   unable to coordinate. However, performing cathodic scans at multiple scan rates and switching

2   potentials provided insight into the mechanism of catalytic CO_2 reduction and the electronic

3   factors impacting catalysis. **Scheme 2** summarizes the proposed electrochemical and chemical

4   processes that lead to catalytic CO_2 reduction. **Figure 6** shows cathodic scans of $[Ru^{II}(tpy)(4,4'-$

5    $(MeO)_2bpy)X]^{n+}$ (**3-Cl** and **3-CH₃CN**) in Ar- and CO_2-saturated acetonitrile solutions with

6   cathodic current enhancements visible at potentials more negative than -1.74 V vs $Fc^{0/+}$ under a

7   CO_2 atmosphere. Qualitatively similar voltammograms are obtained for complexes **1**, **2**, and **4**

8   (**Figures S17-S19**). While previous reports using $[Ru^{II}(tpy)(bpy)NCCH_3]^{2+}$ ascribe this cathodic

9   current enhancement to multiple electron transfer steps within the catalytic cycle for CO_2

10   reduction to CO,[18, 21] the present study gives a more intimate picture of the order of chemical and

11   electrochemical steps, as well as the impact NN ligand donor strength has on catalytic activity.
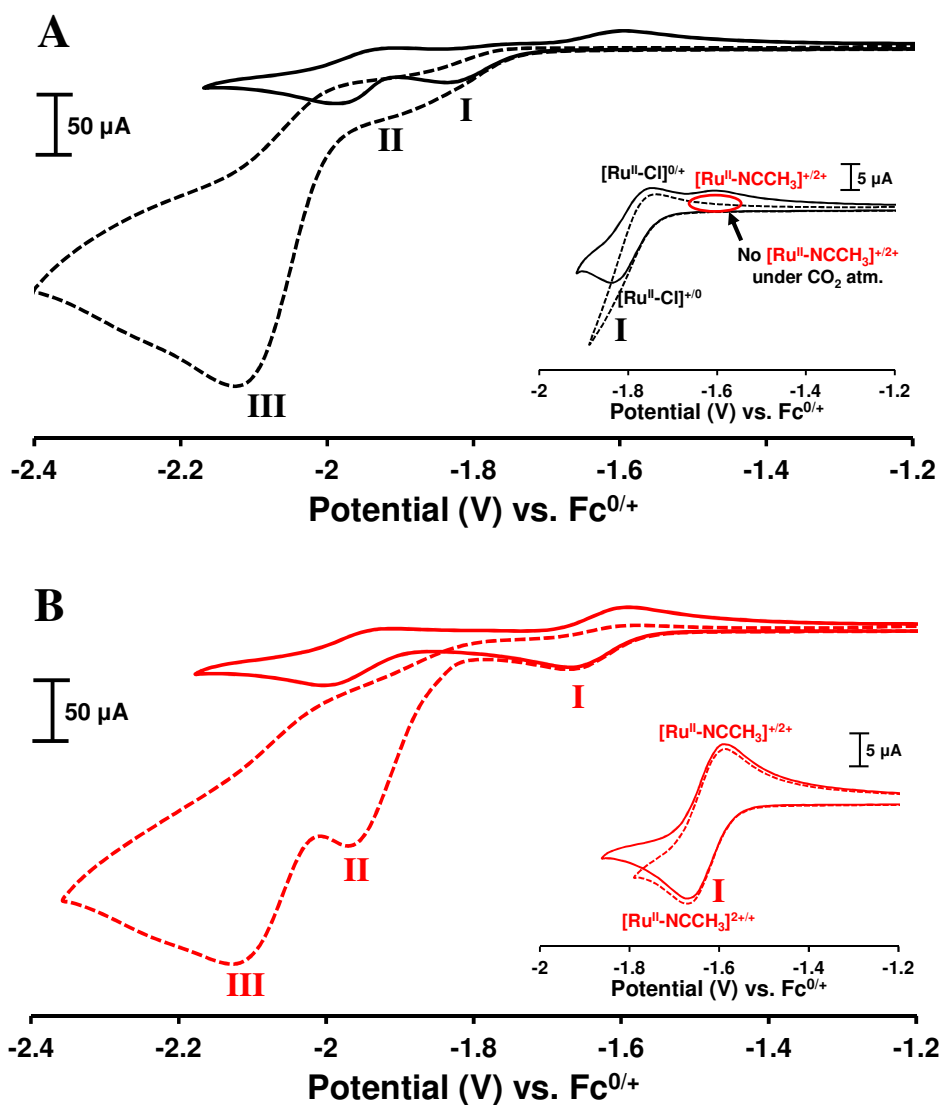
Fig. 6 (**A**) CVs displaying the cathodic region of $[Ru^{II}(tpy)(4,4'-(MeO)_2bpy)Cl]^+$ under Ar (solid black line) and CO_2 (dashed black line) atmospheres at $v = 200$ mV/s. Inset: Isolation of 1st reduction process under Ar (solid) and CO_2 (dashed) atmospheres. (**B**) CVs displaying the cathodic region of $[Ru^{II}(tpy)(4,4'-(MeO)_2bpy)NCCH_3]^{2+}$ under Ar (solid red line) and CO_2 (dashed red line) atmospheres at $v = 200$ mV/s. Inset: Isolation of 1st reduction process under Ar (solid) and CO_2 (dashed) atmospheres.

Comparing the reductive waves for complexes **1**-**4** in the absence and presence of CO_2 allows the detection of processes that arise from CO_2-related chemistry. Analysis of the Cl^- substituted

1   complex under CO_2 is presented first. As shown in **the inset of Figure 6A**, switching scan

2   direction after the one-electron reduction of $[Ru^{II}-Cl]^{+/0}$ (**I**) reveals only $[Ru^{II}-Cl]^{0/+}$ oxidation and

3   an absence of the $[Ru^{II}-NCCH_3]^{+/2+}$ oxidation that was observed in the voltammograms obtained

4   under Ar. This observation is significant and suggests $[Ru^{II}-NCCH_3]^+$ that is partially formed in

5   the one-electron reduction of $[Ru^{II}-Cl]^+$ either reacts further in the presence of CO_2, or that CO_2

6   binds directly to a five-coordinate $[Ru]^+$ intermediate that arises from Cl^- dissociation (**Scheme**

7   **2**). Either way, we ascribe the absence of the anodic wave associated with $[Ru^{II}-NCCH_3]^+$

8   oxidation to the formation of a one-electron reduced, CO_2-adduct $[Ru^{II}-CO_2]^+$. The only

9   remaining feature in the anodic scan following $[Ru^{II}-Cl]^{+/0}$ reduction originates from trivial $[Ru^{II}-$

10 $Cl]^{0/+}$ re-oxidation to regenerate the original species. Current enhancement beyond -1.80 V

11 (cathodic to the reduction wave) should correspond to $[Ru^{II}-CO_2]^{+/0}$ reduction, while the small

12 current magnitude indicates this to be a minor pathway towards formation of the two-electron

13 reduced $[Ru^{II}-CO_2]^0$ complex. The potential range that is observed for the reduction of the CO_2-

14 bound species (*via* the carbon atom) is plausible, as it can be expected to occur at more positive

15 potential than that of the analogous CH_3CN-bound species given the δ^+ character of the CO_2

16 carbon atom. The broad current response between -1.80 V and -2.00 V (**II**) corresponds to slow

17 conversion of the $[Ru^{II}-Cl]^0$ species to $[Ru^{II}-CO_2]^+$ and subsequent reduction to $[Ru^{II}-CO_2]^0$. The

18 lack of a large catalytic wave at -1.89 V, as seen for the $[Ru^{II}-NCCH_3]^{2+}$ complexes (*vide infra*),

19 also suggests that a significant portion of $[Ru^{II}-Cl]^+$ is stable under the reaction conditions. More

20 negative applied potential induces a large catalytic wave at -2.09 V (**III**) that corresponds to a

21 second reduction to $[Ru^{II}-Cl]^-$, followed by Cl^- dissociation, CO_2 coordination and further

22 reduction processes of the thereby generated $[Ru^{II}-CO_2]^0$ species to produce CO and to

23 regenerate the $[Ru^{II}-NCCH_3]^{n+}$ pre-catalyst.[18, 21]

1   In contrast to the behavior observed for $[Ru^{II}\text{-}Cl]^{+}$, the CVs for the one-electron reduction of

2    $[Ru^{II}\text{-}NCCH_3]^{2+}$ (**I**) are identical in the presence and absence of CO_2 (**Figure 6B inset**). This

3   finding indicates that the one-electron reduced $[Ru^{II}\text{-}NCCH_3]^{+}$ is not sufficiently electron rich to

4   initiate CH_3CN substitution by CO_2. Continued negative scanning past -1.74 V displays a

5   catalytic wave at -1.89 V (**II**) whereby the potential and normalized current response vary with

6   scan rate. This process is labeled as a second, one-electron reduction to form $[Ru^{II}\text{-}NCCH_3]^{0}$,

7   followed by CH_3CN dissociation and CO_2 coordination to form $[Ru^{II}\text{-}CO_2]^{0}$ (**Scheme 2**). Given

8   the large, yet unequal, current response between complexes **1-CH$_3$CN** to **4-CH$_3$CN**, some

9   degree of catalysis is occurring. Peak potential corresponding to this catalytic wave varies from

10   -1.93 V for the electron-donating complexes (NN = $(MeO)_2$bpy, Me_2bpy, ^{t}Bu$_2$bpy) to -1.83 V

11   for the intermediary complex (NN = phen) to -1.77 V for the electron-withdrawing complex

12   (NN = bpm). The large catalytic wave at -2.09 V (**III**) in complexes **1-4** is attributed to further

13   complex reduction and ensuing catalysis, as is observed for the $[Ru^{II}\text{-}Cl]^{+}$ complexes. The varied

14   current response at waves **II** and **III** between complexes (i_{cat}) indicate that NN ligand donor

15   strength impacts catalysis, with electron-donating ligands enhancing catalysis. Consequently,

16   complexes possessing stronger electron-donating ligands require a larger negative applied bias

17   for reduction to occur; therefore the expected overpotential (η) for CO_2 reduction will be larger.

18   Recent work by Savéant and co-workers has illustrated the intimate relationship between

19   turnover frequency (TOF) of the catalyst and the overpotential for substrate reduction.[55]

20   Assuming wave **II** to contain catalytic activity further supports this statement as CH_3CN-

21   substituted complexes with stronger donating NN ligands (**1-3**) are reduced at more negative

22   potential and display larger i_{cat} than NN = phen (**4**) or bpm (**5**) complexes.

20
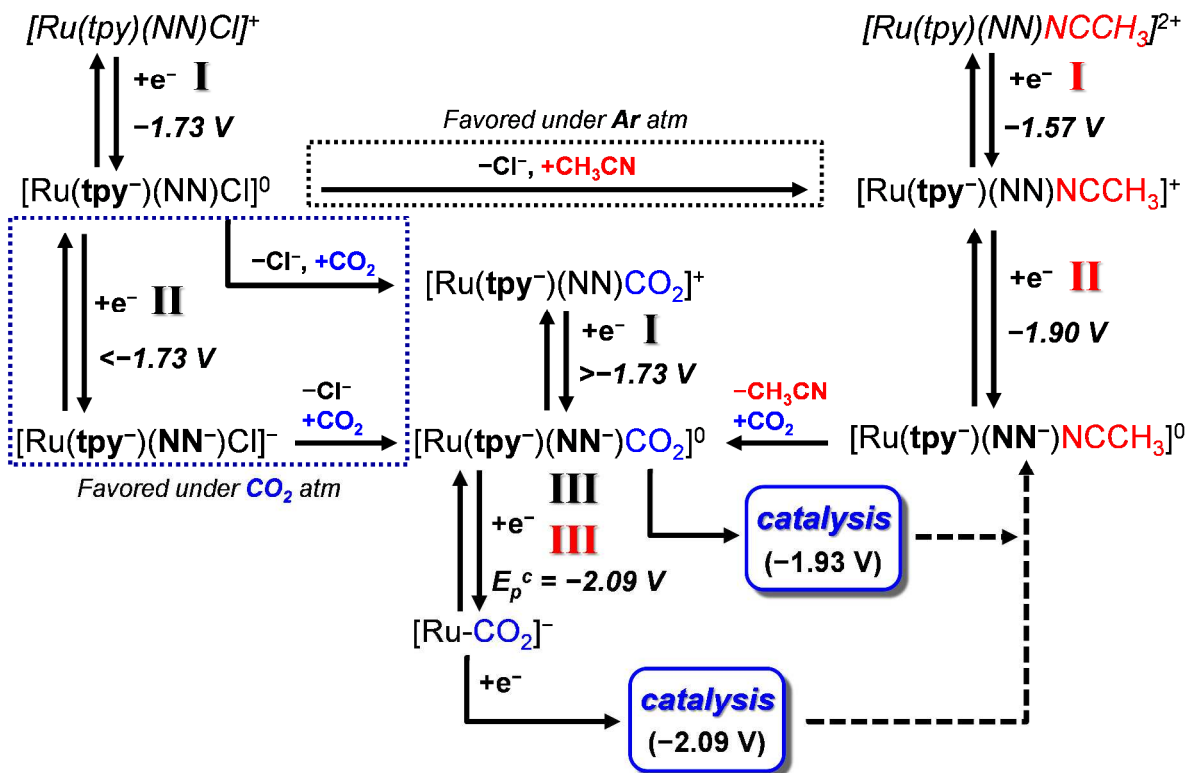
1

2　**Scheme 2** Proposed mechanisms and intermediate species of the electrochemical and chemical

3　processes prior to catalysis in the absence and presence of CO_2 for complexes where the first

4　reduction is tpy(π^*)-based (complexes **1-4**). The specified potentials (vs. $Fc^{0/+}$) correspond to **3-**

5　**Cl** and **3-CH$_3$CN** complexes as an illustrative example and the synthesized complexes are shown

6　in italics.

7　　Decreased electron-density at Ru^{II} *via* bpm or dppz incorporation diminishes CO_2

8　coordination and subsequent catalytic activity as evidenced by the lack of substantial current

9　enhancement in the presence of CO_2, **Figure S20 and S21**. The minimal-to-negligible catalytic

10　activity for this strongly electron-withdrawing architecture emphasizes the need for appropriate

11　energetics to efficiently drive catalysis.

12　　Thorough analysis of all the collected data presents a complex picture as to how electron

13　density at the Ru^{II} center affects the lability and catalytic activity at the sixth coordination site

14　within this molecular architecture. Complexes where the first reduction is primarily tpy(π^*)-

1 based (**1**-**4**) contain NN ligands with a greater degree of electron-donating character as opposed

2 to complexes **5** and **6** where the first reduction is NN(π^*)-based. As described above, the rate

3 constant for Cl^- dissociation correlates well with the degree of electron-donating/withdrawing

4 character, providing knowledge as to how the polypyridyl ligand set influences the lability at the

5 formally Ru^{II} metal center. From a CO_2 reduction viewpoint, complexes with increased electron

6 density at Ru^{II} (Cl^- complexes **1**-**3**) displayed much larger current enhancement ratios when

7 measured under a CO_2 atmosphere vs. an Ar atmosphere (i_{cat}/i_p) than complexes with decreased

8 electron density at Ru^{II} (Cl^- complexes **5** and **6**). Complex **4-Cl** displayed an intermediate

9 current enhancement value compared to the two extremes, as well as possessing a balance of

10 electron-donating and withdrawing character. This observation of catalytic activity as a function

11 of electron density at the formally Ru^{II} metal center is in direct correlation with the rate of Cl^-

12 dissociation through the first reductive couple in $[Ru^{II}(tpy)(NN)Cl]^+$ complexes. By plotting

13 current enhancement under a CO_2 atmosphere (i_{cat}/i_p) vs. the rate constant for Cl^- dissociation

14 (k_{-Cl}), **Figure 8**, the effect of how electron-donating character of the bidentate ligand impacts

15 chemical reactivity and catalytic activity can be seen. Strongly electron-donating polypyridyl

16 ligands increase electron density at Ru^{II} and labilize the Ru-Cl or $Ru-NCCH_3$ bond, thereby

17 producing a coordinatively unsaturated, electron-rich Ru^{II} metal center to coordinate with CO_2.

18 Electron-withdrawing ligands are expected to decrease electron density at Ru^{II} and inhibit

19 efficient reductive, metal-based catalysis.
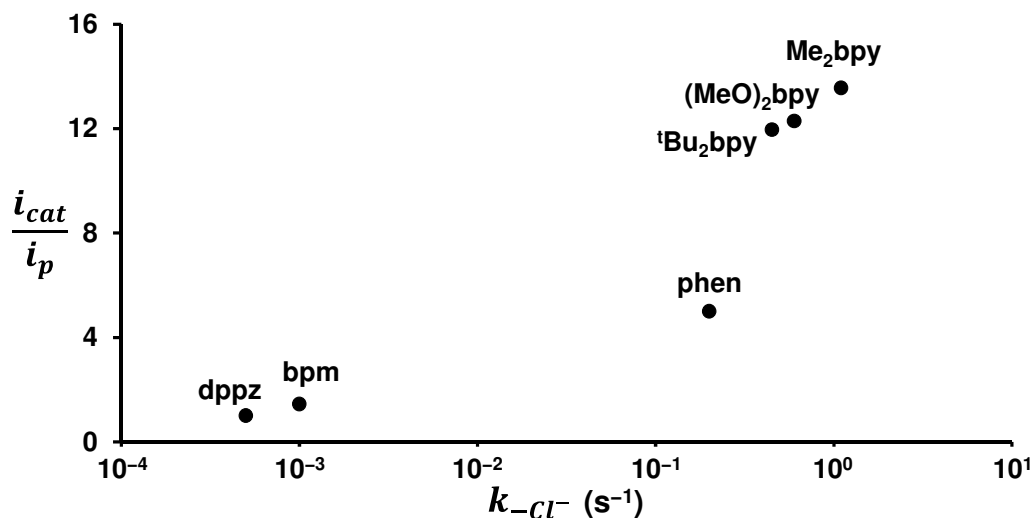
1

2   **Fig. 8** Plot depicting catalytic current enhancement in the presence of CO_2 (i_{cat}/i_p) vs. the rate

3   constant for Cl^- ligand dissociation (k_{-Cl}) in $[Ru^{II}(tpy)(NN)Cl]^+$ complexes where the degree of

4   electron-donating ability of NN varies. Using the chloro-substituted complexes, the i_{cat} values

5   were obtained from the large current response at -2.10 V vs. $Fc^{0/+}$ in the presence of CO_2 and the

6   i_p values were obtained from the current response of the 2nd cathodic wave near -2.0 V vs. $Fc^{0/+}$

7   in the absence of CO_2.

8   **Conclusions**

9   The relative ease of synthesis and purification for this $[Ru^{II}(tpy)(NN)X]^{n+}$ molecular

10   architecture permitted generation of a small library of complexes with varying degrees of

11   electron-donating/withdrawing ability to study their electrochemical and electrocatalytic

12   properties. Isolating the redox couples throughout the cathodic region for $[Ru^{II}-Cl]^+$ and $[Ru^{II}-$

13   $NCCH_3]^{2+}$ complexes display how the rate of monodentate ligand dissociation is directly related

14   to electron density at the formally Ru^{II} metal center through electron donation from the bidentate

15   ligand. This observation is in direct correlation with the reactivity at the sixth coordination site

16   on Ru^{II} as catalytic activity for CO_2 reduction (measured by the ratio of current response in

17   presence and absence of CO_2, i_{cat}/i_p) correlates well with the rate constant for Cl^- ligand

23

1   dissociation (k_{-Cl}). As shown, complexes **1**-**3** where the bidentate ligand contains electron-

2   donating substituents (methyl, *tert*-butyl, methoxy) possess a much larger value for k_{-Cl} and i_{cat}/i_p

3   compared to analogous complexes (**5** and **6**) containing electron-withdrawing components

4   (pyrimidines, phenazine). The phenanthroline-containing complex **4** presented intermediate

5   values for k_{-Cl} and i_{cat}/i_p which indicates the unique properties of the phenanthroline ligand that

6   does not appear to function as either a strong electron-donating or -withdrawing species.

7   Interestingly, $[Ru^{II}\text{-}Cl]^+$ complexes where the first reduction was tpy(π^*)-based (**1**-**4**) showed that

8   after one-electron reduction under CO_2 atmosphere, none of the corresponding CH_3CN-bound

9   species was present upon switching scan direction. While the CH_3CN-bound complex was

10   observed under an argon atmosphere, this lack of $[Ru^{II}\text{-}NCCH_3]^{+/2+}$ oxidation upon scan

11   direction reversal suggests that CO_2 is able to coordinate after one-electron reduction of $[Ru^{II}\text{-}$

12    $Cl]^+$. This unique finding proposes that at least two mechanistic pathways towards CO_2 reduction

13   are present within this architecture and differ by the order of electrochemical vs. chemical steps

14   (i.e. EC vs. CE processes). Such observations of varying mechanisms towards catalysis have

15   been shown to exist for proton and CO_2 reduction using various transition metal-based

16   catalysts.[56, 57] Ongoing studies within the lab involve incorporating this architecture into

17   heterogeneous systems for electrocatalysis, as well as utilizing the strong light absorbing nature

18   and catalytic activity for CO_2 reduction of this $[Ru^{II}(NNN)(NN)X]^{n+}$ motif for photocatalytic

19   systems.

20

21   **Supporting Information**. Electronic absorption spectra, cyclic voltammograms, and ^{1}H-NMR

22   spectra of complexes. This material is available free of charge *via* the Internet at

23   http://pubs.acs.org.

1   **Corresponding Author**

2   *sascha.ott@kemi.uu.se

3   **Notes**

4   The authors declare no competing financial interest.

10   REFERENCES

1.   C. D. Windle and R. N. Perutz, *Coord. Chem. Rev.*, 2012, **256**, 2562-2570.
2.   B. Kumar, M. Llorente, J. Froehlich, T. Dang, A. Sathrum and C. P. Kubiak, *Annu. Rev. Phys. Chem.*, 2012, **63**, 541-+.
3.   J. L. Inglis, B. J. MacLean, M. T. Pryce and J. G. Vos, *Coord. Chem. Rev.*, 2012, **256**, 2571-2600.
4.   A. J. Morris, G. J. Meyer and E. Fujita, *Acc. Chem. Res.*, 2009, **42**, 1983-1994.
5.   C. Costentin, M. Robert and J.-M. Saveant, *Chem. Soc. Rev.*, 2013, **42**, 2423-2436.
6.   E. E. Benson, C. P. Kubiak, A. J. Sathrum and J. M. Smieja, *Chem. Soc. Rev.*, 2009, **38**, 89-99.
7.   J. Schneider, H. Jia, J. T. Muckerman and E. Fujita, *Chem. Soc. Rev.*, 2012, **41**, 2036-2051.
8.   J. Schneider, H. Jia, K. Kobiro, D. E. Cabelli, J. T. Muckerman and E. Fujita, *Energy Environ. Sci.*, 2012, **5**, 9502-9510.
9.   J. D. Froehlich and C. P. Kubiak, *Inorg. Chem.*, 2012, **51**, 3932-3934.
10.   B. J. Fisher and R. Eisenberg, *J. Am. Chem. Soc.*, 1980, **102**, 7361-7363.
11.   C. Costentin, S. Drouet, M. Robert and J.-M. Savéant, *Science*, 2012, **338**, 90-94.
12.   I. Bhugun, D. Lexa and J.-M. Savéant, *J. Am. Chem. Soc.*, 1996, **118**, 1769-1776.
13.   P. Kang, C. Cheng, Z. Chen, C. K. Schauer, T. J. Meyer and M. Brookhart, *J. Am. Chem. Soc.*, 2012, **134**, 5500-5503.
14.   J. W. Raebiger, J. W. Turner, B. C. Noll, C. J. Curtis, A. Miedaner, B. Cox and D. L. DuBois, *Organometallics*, 2006, **25**, 3345-3351.
15.   D. L. DuBois, A. Miedaner and R. C. Haltiwanger, *J. Am. Chem. Soc.*, 1991, **113**, 8753-8764.
16.   S. Slater and J. H. Wagenknecht, *J. Am. Chem. Soc.*, 1984, **106**, 5367-5368.

17. Y. Matsubara, S. E. Hightower, J. Chen, D. C. Grills, D. E. Polyansky, J. T. Muckerman, K. Tanaka and E. Fujita, *Chem. Commun.*, 2014, **50**, 728-730.
18. Z. Chen, P. Kang, M.-T. Zhang and T. J. Meyer, *Chem. Commun.*, 2014, **50**, 335-337.
19. M. Bourrez, M. Orio, F. Molton, H. Vezin, C. Duboc, A. Deronzier and S. Chardon-Noblat, *Angew. Chem., Int. Ed.*, 2014, **53**, 240-243.
20. J. M. Smieja, M. D. Sampson, K. A. Grice, E. E. Benson, J. D. Froehlich and C. P. Kubiak, *Inorg. Chem.*, 2013, **52**, 2484-2491.
21. Z. Chen, C. Chen, D. R. Weinberg, P. Kang, J. J. Concepcion, D. P. Harrison, M. S. Brookhart and T. J. Meyer, *Chem. Commun.*, 2011, **47**, 12607-12609.
22. M. Bourrez, F. Molton, S. Chardon-Noblat and A. Deronzier, *Angew. Chem., Int. Ed.*, 2011, **50**, 9903-9906.
23. J. M. Smieja and C. P. Kubiak, *Inorg. Chem.*, 2010, **49**, 9283-9289.
24. S. C. Rasmussen, M. M. Richter, E. Yi, H. Place and K. J. Brewer, *Inorg. Chem.*, 1990, **29**, 3926-3932.
25. C. M. Bolinger, N. Story, B. P. Sullivan and T. J. Meyer, *Inorg. Chem.*, 1988, **27**, 4582-4587.
26. H. Ishida, K. Tanaka and T. Tanaka, *Organometallics*, 1987, **6**, 181-186.
27. B. P. Sullivan, C. M. Bolinger, D. Conrad, W. J. Vining and T. J. Meyer, *J. Chem. Soc., Chem. Commun.*, 1985, 1414-1416.
28. J. Hawecker, J.-M. Lehn and R. Ziessel, *J. Chem. Soc., Chem. Commun.*, 1984, 328-330.
29. M. D. Sampson, A. D. Nguyen, K. A. Grice, C. E. Moore, A. L. Rheingold and C. P. Kubiak, *J. Am. Chem. Soc.*, 2014, **136**, 5460-5471.
30. J. M. Smieja, E. E. Benson, B. Kumar, K. A. Grice, C. S. Seu, A. J. M. Miller, J. M. Mayer and C. P. Kubiak, *Proc. Natl. Acad. Sci. U. S. A.*, 2012, **109**, 15646-15650.
31. H. W. Tseng, R. Zong, J. T. Muckerman and R. Thummel, *Inorg. Chem.*, 2008, **47**, 11763-11773.
32. D. J. Wasylenko, C. Ganesamoorthy, B. D. Koivisto, M. A. Henderson and C. P. Berlinguette, *Inorg. Chem.*, 2010, **49**, 2202-2209.
33. D. J. Wasylenko, C. Ganesamoorthy, M. A. Henderson, B. D. Koivisto, H. D. Osthoff and C. P. Berlinguette, *J. Am. Chem. Soc.*, 2010, **132**, 16094-16106.
34. S. Maji, I. López, F. Bozoglian, J. Benet-Buchholz and A. Llobet, *Inorg. Chem.*, 2013, **52**, 3591-3593.
35. J. J. Concepcion, M.-K. Tsai, J. T. Muckerman and T. J. Meyer, *J. Am. Chem. Soc.*, 2010, **132**, 1545-1557.
36. J. J. Concepcion, J. W. Jurss, J. L. Templeton and T. J. Meyer, *J. Am. Chem. Soc.*, 2008, **130**, 16462-16463.
37. J. J. Concepcion, J. W. Jurss, M. R. Norris, Z. Chen, J. L. Templeton and T. J. Meyer, *Inorg. Chem.*, 2010, **49**, 1277-1279.
38. N. Kaveevivitchai, R. Zong, H.-W. Tseng, R. Chitta and R. P. Thummel, *Inorg. Chem.*, 2012, **51**, 2930-2939.
39. Z. Chen, C. R. K. Glasson, P. L. Holland and T. J. Meyer, *Phys. Chem. Chem. Phys.*, 2013, **15**, 9503-9507.
40. H. Konno, A. Kobayashi, K. Sakamoto, F. Fagalde, N. E. Katz, H. Saitoh and O. Ishitani, *Inorg. Chim. Acta*, 2000, **299**, 155-163.
41. H. Nagao, T. Mizukawa and K. Tanaka, *Inorg. Chem.*, 1994, **33**, 3415-3420.

42. A. Greguric, I. D. Greguric, T. W. Hambley, J. R. Aldrich-Wright and J. G. Collins, *J. Chem. Soc., Dalton Trans.*, 2002, 849-855.
43. B. P. Sullivan, J. M. Calvert and T. J. Meyer, *Inorg. Chem.*, 1980, **19**, 1404-1407.
44. P. A. Adcock, F. R. Keene, R. S. Smythe and M. R. Snow, *Inorg. Chem.*, 1984, **23**, 2336-2343.
45. S. Bonnet, J.-P. Collin, N. Gruber, J.-P. Sauvage and E. R. Schofield, *Dalton Trans.*, 2003, 4654-4662.
46. S. Swavey, Z. Fang and K. J. Brewer, *Inorg. Chem.*, 2002, **41**, 2598-2607.
47. N. Gupta, N. Grover, G. A. Neyhart, W. Liang, P. Singh and H. H. Thorp, *Angew. Chem., Int. Ed.*, 1992, **31**, 1048-1050.
48. M. Frasconi, Z. Liu, J. Lei, Y. Wu, E. Strekalova, D. Malin, M. W. Ambrogio, X. Chen, Y. Y. Botros, V. L. Cryns, J.-P. Sauvage and J. F. Stoddart, *J. Am. Chem. Soc.*, 2013, **135**, 11603-11613.
49. H. E. Gottlieb, V. Kotlyar and A. Nudelman, *J. Org. Chem.*, 1997, **62**, 7512-7515.
50. A. Gennaro, A. A. Isse and E. Vianello, *J. Electroanal. Chem.*, 1990, **289**, 203-215.
51. M. N. Ackermann and L. V. Interrante, *Inorg. Chem.*, 1984, **23**, 3904-3911.
52. M. Maestri, N. Armaroli, V. Balzani, E. C. Constable and A. M. W. C. Thompson, *Inorg. Chem.*, 1995, **34**, 2759-2767.
53. D. P. Rillema, G. Allen, T. J. Meyer and D. Conrad, *Inorg. Chem.*, 1983, **22**, 1617-1622.
54. Y. Matsubara, E. Fujita, M. D. Doherty, J. T. Muckerman and C. Creutz, *J. Am. Chem. Soc.*, 2012, **134**, 15743-15757.
55. C. Costentin, S. Drouet, M. Robert and J.-M. Savéant, *J. Am. Chem. Soc.*, 2012, **134**, 11235-11242.
56. D. L. DuBois, *Inorg. Chem.*, 2014, **53**, 3935-3960.
57. S. Tschierlei, S. Ott and R. Lomoth, *Energy Environ. Sci.*, 2011, **4**, 2340-2352.

Synopsis and TOC
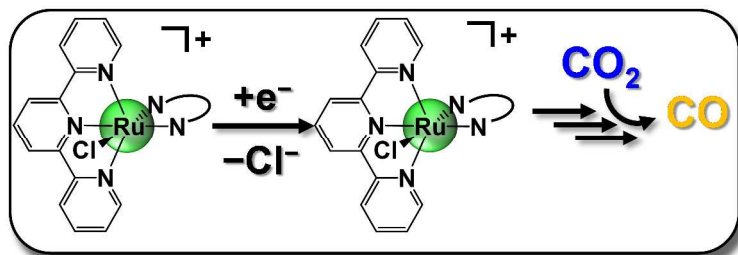
Modifying the electron density within a Ru^{II}-polypyridyl molecular architecture *via* electron-donating/withdrawing character of the bidentate ligand set has provided insight into the electronic requirements for catalytic CO_2 reduction.